

# Formation of Bio-based Derived Dicalcium Silicate Ceramics via Mechanochemical Treatment: Physical, XRD, SEM and FTIR Analyses

Siti Nur Hazwani Yunus<sup>1</sup>, Khor Shing Fhan<sup>1,2\*</sup>, Banjuraizah Johar<sup>3</sup>, Nur Maizatul Shima Adzali<sup>3</sup>, Nur Hazlinda Jakfar<sup>3</sup>, Cheng Ee Meng<sup>4,5</sup>, Emma Ziezie Mohd Tarmizi<sup>6</sup>, Zainal Abidin Talib<sup>7</sup>

<sup>1</sup> Faculty of Electrical Engineering & Technology, Universiti Malaysia Perlis (UniMAP), Perlis, Malaysia.

<sup>2</sup> Centre of Excellence for Renewable Energy (CERE), Universiti Malaysia Perlis (UniMAP), Perlis, Malaysia.

<sup>3</sup> Faculty of Chemical Engineering & Technology, Universiti Malaysia Perlis (UniMAP), Perlis, Malaysia.

<sup>4</sup> Advanced Communication Engineering, Centre of Excellence (ACE), Universiti Malaysia Perlis (UniMAP), Perlis, Malaysia.

<sup>5</sup> Faculty of Electronic Engineering & Technology, Universiti Malaysia Perlis (UniMAP), Perlis, Malaysia.

<sup>6</sup> Centre of Foundation Studies for Agricultural Science, Universiti Putra Malaysia UPM, 43400, Serdang, Selangor, Malaysia.

<sup>7</sup> Department of Physics, College of Natural Sciences, Jeonbuk National University 567, Baekje-daero, Deokjin-gu, Jeonju-si, Jeollabuk-do, 54896 Republic of Korea.

Received 26 August 2022, Revised 14 October 2022, Accepted 26 October 2022

## ABSTRACT

Beta-dicalcium silicate plays an important role in modern technology, but its tendency for polymorphic transformation results in the dusting phenomenon, is a major challenge. Therefore, mechanochemical treatment is used to reduce the particle size to retain the stability of the polymorph. In this study, pure dicalcium silicate ceramics of  $\beta$ -monoclinic structure with P 121/c1 space group were synthesized using calcium oxide and silicate powders derived from calcined eggshells and rice husks, respectively. The powders were mixed in a 2:1 molar ratio by mechanochemical treatment and heat-treated in the air at temperatures ranging from 900°C to 1100°C for 2 h. The results reveal that pure beta-dicalcium silicate formed at 1100°C without adding stabilizers. The properties of the pristine and sintered bodies were characterized by X-ray diffraction (XRD), Fourier transform infrared (FTIR) spectroscopy, and scanning electron microscopy (SEM). SEM revealed that the grain and pore sizes increase with rising sintering temperatures. FTIR spectra indicate the existence of Si-O bonds in  $\text{SiO}_4$  tetrahedrons on all the samples. The sample sintered at 1000°C attains the lowest bulk density (1.2463 g/cm<sup>3</sup>), whereas the apparent porosity is the highest (62.5%). The reason for this trend is due to the decomposition of carbonate into CO<sub>2</sub> gas. The densification onset for the sample sintered at 1100°C as the bulk density rises and grain size achieves 6.06  $\mu\text{m}$ . This study further explains the effect of sintering temperatures on the physical, structural, and morphological properties of Ca<sub>2</sub>SiO<sub>4</sub> which would also be useful for further optimization of its use.

**Keywords:** Dicalcium silicate, Sintering, Morphology, X-ray Diffraction, Porosity

## 1. INTRODUCTION

Dicalcium silicate (Ca<sub>2</sub>SiO<sub>4</sub>) is unique in that it exhibits hydrability and complex polymorphism, resulting in polymorphic forms ( $\alpha$ ,  $\beta$ , or  $\gamma$ ) with distinct physical and chemical properties [1] at different processing temperatures. Chemical stabilization was typically regarded as the most

\* Corresponding author: sfkhor@unimap.edu.my

crucial component in dicalcium silicate for maintaining the high-temperature P-phase down to ambient temperature [2]. These characteristics find a wide range of applications in cementitious materials [3], refractory materials [4], coating materials [5], and ceramic and biological materials [6,7,8,9]. The potential applications of dicalcium silicate have been the subject of continuous research [3,10,11,12,13].

$\text{Ca}_2\text{SiO}_4$  is usually obtained by mixing several chemical solutions and has been prepared by various approaches, such as the sol-gel process [5,6,14,15,16], Pechini method [17,18], combustion method [19], aerosol flame [20], hydrothermal synthesis [21], spark plasma sintering [22] using chemical reagent grade calcium nitrate tetrahydrate, and solid-state reaction [23] using ethanol during milling. The procedure and the apparatus for these processes are complicated, which is not suitable and unsustainable for the mass production of  $\text{Ca}_2\text{SiO}_4$ . A previous work [24] reported the effectiveness of using eggshells as a synthetic raw material for the synthesis of  $\text{Ca}_2\text{SiO}_4$  by a sol-gel combustion technique. However, it has been established that  $\text{Ca}_2\text{SiO}_4$  samples often crack or undergo “dusting” phenomena, resulting in damaged and unusable samples. Thus, stabilizers are commonly used to stabilize the form of  $\text{Ca}_2\text{SiO}_4$  [25,26,27,28,29,30]. Nevertheless, Chrysafi *et al.* [16] obtained  $\beta\text{-Ca}_2\text{SiO}_4$  without any chemical stabilizer through hydrosol-gel and non-aqueous sol-gel methods.

In the present study, a mechanochemical route was used for the synthesis of  $\beta\text{-Ca}_2\text{SiO}_4$  due to its advantages of simplicity, low cost, and yielding highly pure products. Therefore,  $\beta\text{-Ca}_2\text{SiO}_4$  was synthesized via the mechanochemical route without using stabilizers and followed by heat treatment. These starting powders, *i.e.*, calcium oxide and silica, are derived from calcined eggshells and rice husks, respectively, which also directly relieve environmental pressure. As a result, pure  $\beta\text{-Ca}_2\text{SiO}_4$  ceramics were obtained after the mixed powder was sintered at 1100°C for 2 h. The results were explained in terms of the mechanochemical reaction that generates higher surface areas for the starting powders to interact and form pure  $\beta\text{-Ca}_2\text{SiO}_4$  without the dusting phenomenon. Additionally, the effect of sintering temperature on the physical and morphology properties of the samples was investigated.

## 2. MATERIAL AND METHODS

Raw rice husks were obtained from a rice mill factory in the northern region of Malaysia, while eggshells were obtained from daily basis food waste. Both of the materials were cleaned and dried before the calcination process. Powder for preparing pristine samples was treated via mechanochemical techniques. Raw eggshell (RES) and raw rice husk (RRH) were used as the starting materials to yield a white powder of CaO and  $\text{SiO}_2$  by calcining at 900°C and 800°C, respectively. The CaO and  $\text{SiO}_2$  powders were carefully weighed in a ratio of 2:1 according to the stoichiometric calculation, and the powder was mixed and ball-milled for 10 h by using high-energy planetary ball milling with tungsten carbide balls as the milling medium. The milled mixtures were subsequently compacted into a disk-shape pallet of 12 mm diameter by using a uniaxial hydraulic press and sintered at 900 °C, 1000 °C, and 1100 °C for 2 h with a heating rate of 5 °C/min.

By utilizing dynamic light scattering, Malvern Zetasizer nano-zs (Malvern Instruments Ltd., U.K.) was employed to ascertain the particle size distribution of the RES, CES, and milled mixture. This method uses the Stokes-Einstein connection to translate the diffusion of particles moving with Brownian motion into their size and size distribution.

Energy Dispersive X-ray Fluorescence (EDXRF, PAN analytical MiniPAL 4) was used to quantitatively determine the chemical compositions that are present in these powder materials, except for the lightest elements. The thermal behavior of the precursor was determined using the Mettler Toledo model TGA/DSC 2 HT at a heating rate of 5 °C/min from 30 °C until 1200 °C. The phase analysis was carried out using XRD (Bruker D2 Phaser Model) collected over a scan range of 10° to 90° 2θ at a scan speed of 2° 2θ/min, and a step size of 0.02° 2θ with CuKα radiation (Kα = 1.5406 nm) at 10 mA and 30 kV. Identification of phases was achieved by comparing the resultant diffraction patterns with the ICSD (JCPDS) standard. Xpert-Highscore Plus software was used.

Perkin Elmer FTIR Spectrum RXI Spectrometer was used to determine the functional groups that existed in the sample powders. The FTIR spectra were obtained in transmittance mode from 400 cm<sup>-1</sup> –4000 cm<sup>-1</sup> at a resolution of 1 cm<sup>-1</sup>. Scanning electron microscopy (SEM, JEOL Model JSM-6450LA) has been used for the morphological study of pristine and sintered samples. The samples were platinum-coated by the spin coating technique and mounted on the SEM sample stage with conductive double-sided carbon tape before SEM imaging. The average grain and pore size of the sintered specimens were determined from SEM images using the linear intercept approach [31,32,33].

The bulk densities of the pristine and sintered samples were identified using the Archimedes principle. This procedure was carried out using the standard test methods of ISO 5017, ASTM C20, and BS 1902-308 [34]. On the other hand, the percentage of volume shrinkage was calculated using the following expression:

$$\text{Volume shrinkage (\%)} = [(V_o - V)/V_o] \times 100 \quad (1)$$

where V<sub>o</sub> and V are the volume of the sample specimen before and after the sintering process, respectively.

### 3. RESULTS AND DISCUSSION

#### 2.6 Elemental Analysis

The chemical composition of chicken eggshell and rice husk in the raw and calcined stages was measured by XRF and tabulated in Tables 1 and 2, respectively. The raw chicken eggshell (RES) is mainly composed of calcium carbonate, CaCO<sub>3</sub> at 98.3wt%, and other oxide compounds at 1.7wt%. After calcination at 900 °C, the calcined chicken eggshell (CES) is composed of calcium oxide, CaO of 96.23wt%, and other compounds of 3.87wt%. The results obtained were similar to [35] where they also obtained less weight in the percentage of CaO in calcined eggshells compared to CaCO<sub>3</sub> in raw eggshells. On the other hand, the weight percentage of silica, SiO<sub>2</sub> increased from 56.3wt% in raw rice husks (RRH) to 91.7wt% in calcined rice husks (CRH) with a lower impurity of 8.3wt% after calcination. Since natural materials are used as precursors, other elements are also present in powders at a low percentage.

**Table 1** Percentage of chemical compositions exist in raw and calcined eggshells.

| RES     |       | CES     |       |
|---------|-------|---------|-------|
| Element | %     | Element | %     |
| CaO     | 98.30 | CaO     | 96.23 |

|                                |       |                                |       |
|--------------------------------|-------|--------------------------------|-------|
| MgO                            | 0.735 | Na <sub>2</sub> O              | 2.400 |
| K <sub>2</sub> O               | 0.310 | MgO                            | 0.580 |
| Al <sub>2</sub> O <sub>3</sub> | 0.252 | Al <sub>2</sub> O <sub>3</sub> | 0.200 |
| P <sub>2</sub> O <sub>5</sub>  | 0.167 | RuO <sub>2</sub>               | 0.200 |
| SO <sub>3</sub>                | 0.086 | SO <sub>3</sub>                | 0.100 |
| SrO                            | 0.045 | Nd <sub>2</sub> O <sub>3</sub> | 0.100 |
| Cl                             | 0.036 | Cu <sub>3</sub> O <sub>4</sub> | 0.080 |
| BaO                            | 0.029 | SrO                            | 0.058 |
| Cs <sub>2</sub> O              | 0.020 | Cu <sub>3</sub> O <sub>4</sub> | 0.032 |
|                                |       | Sm <sub>2</sub> O <sub>3</sub> | 0.030 |
|                                |       | Yb <sub>2</sub> O <sub>3</sub> | 0.030 |
|                                |       | ZrO <sub>2</sub>               | 0.015 |

**Table 2** Percentage of chemical compositions exist in raw and calcined rice husk.

| RRH                            |       | CRH                            |       |
|--------------------------------|-------|--------------------------------|-------|
| Element                        | %     | Element                        | %     |
| SiO <sub>2</sub>               | 56.30 | SiO <sub>2</sub>               | 91.70 |
| K <sub>2</sub> O               | 17.70 | K <sub>2</sub> O               | 5.880 |
| Na <sub>2</sub> O              | 10.00 | CaO                            | 1.580 |
| MgO                            | 5.350 | MnO                            | 0.252 |
| CaO                            | 2.900 | Fe <sub>2</sub> O <sub>3</sub> | 0.171 |
| P <sub>2</sub> O <sub>5</sub>  | 2.160 | CuO                            | 0.067 |
| Al <sub>2</sub> O <sub>3</sub> | 1.500 | ZnO                            | 0.043 |
| SO <sub>3</sub>                | 1.280 | As <sub>2</sub> O <sub>2</sub> | 0.006 |
| Fe <sub>2</sub> O <sub>3</sub> | 0.939 | Rb <sub>2</sub> O              | 0.018 |
| Cl                             | 0.827 | PdO                            | 0.120 |
| MnO                            | 0.366 | Eu <sub>2</sub> O <sub>3</sub> | 0.070 |
| Cr <sub>2</sub> O <sub>3</sub> | 0.209 | Re <sub>2</sub> O <sub>7</sub> | 0.037 |
| NiO                            | 0.096 | OsO <sub>4</sub>               | 0.009 |
| ZnO                            | 0.082 | PbO                            | 0.020 |
| V <sub>2</sub> O <sub>5</sub>  | 0.068 |                                |       |
| CuO                            | 0.046 |                                |       |
| TiO <sub>2</sub>               | 0.030 |                                |       |
| CdO                            | 0.017 |                                |       |
| Rb <sub>2</sub> O              | 0.017 |                                |       |
| Br                             | 0.016 |                                |       |
| Ag <sub>2</sub> O              | 0.016 |                                |       |
| PbO                            | 0.012 |                                |       |

### 3.2 Particle size analysis

The particle size distribution curve of the produced RES, CES, and the milled mixture powder is presented in Fig. 1. In Fig. 1, the particle size distribution of CES powder exhibits a bimodal characteristic. It shows that some of the unmilled coarse particles form a mode towards the largest particle size, while fractured smaller particles produce a new mode that manifests at a smaller size range. Hence, the main peak, i.e., a large fraction of particles with a diameter ~413.2 nm was detected. Meanwhile, the presence of some smaller particles is detected around 132.2 nm. Next, the particle size distribution of CRH powder has a normal distribution curve, indicating the size distribution is fully symmetrical. The main peak particle size distribution detected is at 122.8 nm. Fig. 1 also depicts the particle size distribution of the milled mixture powder that has been ground through ball milling for 10 h. The particle size distributions were unimodal, but the main peak particle size distribution was found to significantly increase to 801.5 nm. The particle size of powder increases after milling treatment, as also reported in [36]. The milled mixture powders exhibited larger particle sizes, probably due to the prolonged

impact of the grinding media against the walls of the milling jar, which caused very fine particles to restack to form larger powder agglomerates. In other words, milling treatment effectively reduces particle sizes and increases the surface contact area between the particles. In addition, the Van Der Waals forces between the surfaces of fine powder are stronger than the powder's gravitational mass, which causes the powder agglomeration [37]. In short, more surface area results in greater Van Der Waals forces, which strengthen the attraction between particles [38].

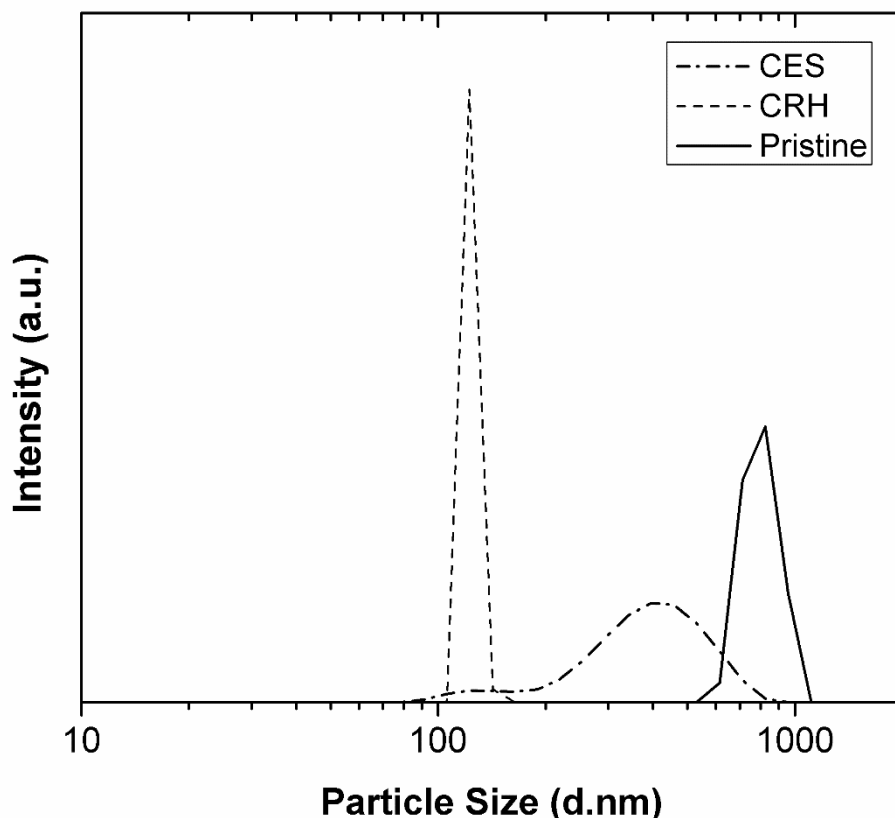


**Fig. 1.** Particle size distribution of calcine eggshells (CES), calcine rice husk (CRH), and the milled mixture (pristine) powders.

### 3.3 Thermal property analysis

Thermogravimetric – Differential Thermal Analysis (TGA-DTA) analysis was conducted to study the thermal stability of the mixture powders. The TGA and DTA results for the pristine body are shown in Fig. 2. A slight weight loss of 3.85% and an exothermic peak below 400°C were induced by free evaporable water [39]. The smaller weight loss of 3.27% and the first endothermic peak occurred between 420 °C and 480 °C corresponding to poor crystalline calcium carbonate [40], whereas the weight loss of 26.88% and larger endothermic peak between 480 °C and 720°C were attributed to well-crystallized calcite decarbonization [40]. Hence, TGA analysis showed a total weight loss of 34% for the mixture powders.

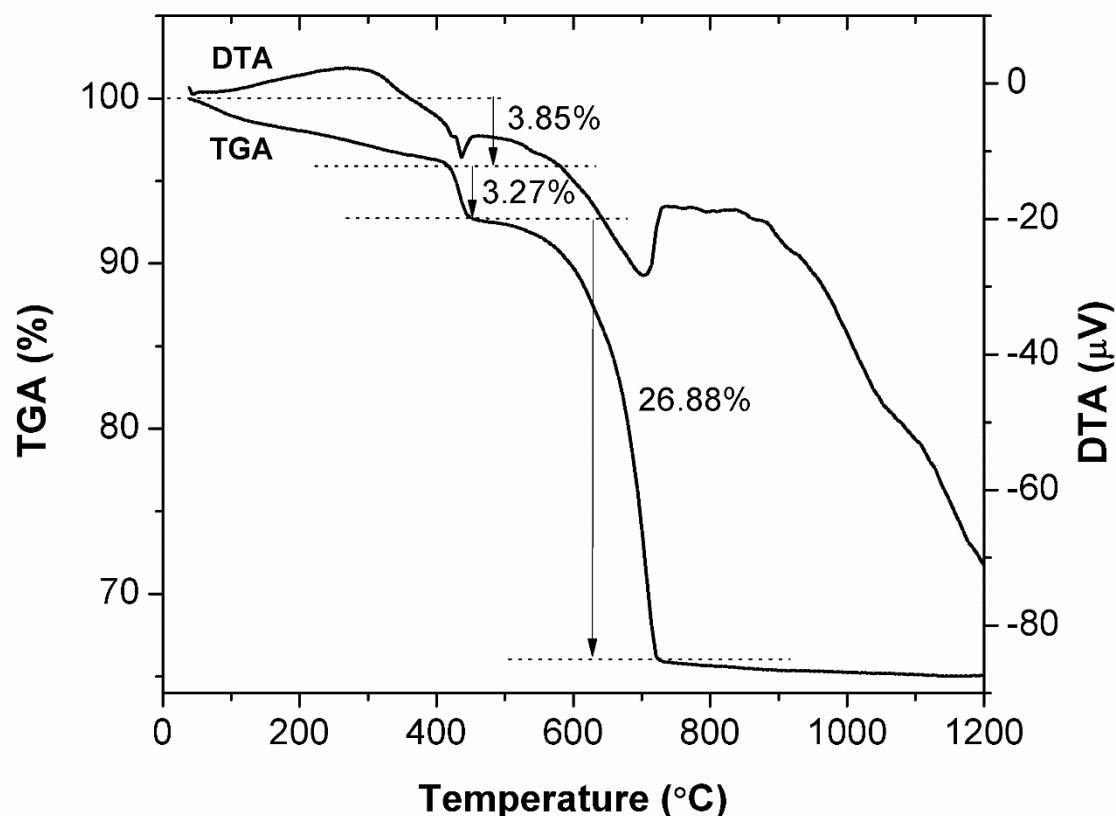


Fig. 2. TGA/DTA illustration of pristine body.

### 3.4 Structural analysis

Fig. 3 depicts the XRD patterns of the pristine sample and sintered samples at 900 °C, 1000 °C, and 1100 °C. All samples reveal quite similar diffraction profiles and crystal structures formed by  $\text{Ca}_2\text{SiO}_4$  exhibited in polycrystalline  $\beta$ -monoclinic structures. The XRD pattern in Fig. 3 shows sharp and well-defined diffraction, indicating that the milled powder from the mechanochemical process has a degree of crystallinity at a long range of  $\beta$ - $\text{Ca}_2\text{SiO}_4$  and  $\text{SiO}_2$ . XRD analysis revealed that the major phase is larnite,  $\beta$ - $\text{Ca}_2\text{SiO}_4$ , with a small amount of silica,  $\text{SiO}_2$ . The mechanochemical treatment of the mixed powders yielded very fine homogeneous powders [41], which enhanced the reactivity between the corresponding single-phase  $2\text{CaO}$  and  $1\text{SiO}_2$  compounds to form  $\text{Ca}_2\text{SiO}_4$ . The phase of  $\text{SiO}_2$  remains present at sintering temperatures of 900°C and 1000°C, as shown in Fig. 3. From Table 3, it is observed that the percentage of  $\beta$ - $\text{Ca}_2\text{SiO}_4$  in the sintered samples increases as sintering temperatures rise, and it varies from 82.9% to 96.9% for the pristine body to 1000 °C. The sample sintered at 1100 °C has shown a single phase, i.e., 100%  $\beta$ - $\text{Ca}_2\text{SiO}_4$  without an impurity phase. In short, the sintering process at 1100°C of the mixture of  $2\text{CaO}$  and  $1\text{SiO}_2$  extracted from chicken eggshells and rice husks can synthesize pure  $\text{Ca}_2\text{SiO}_4$  without using stabilizers. Moreover, the sintering temperature used is lower than 1250°C for 8 h as applied in previous works [42,43]. Furthermore, the pristine body and sintered samples are stable at room temperature and never undergo the dusting phenomenon. The stability of the  $\beta$ - $\text{Ca}_2\text{SiO}_4$  may be attributed to the small particle size obtained from the mechanochemical treatment. The particle size of  $\beta$ - $\text{Ca}_2\text{SiO}_4$  within 1 – 3  $\mu\text{m}$  [16] and 5 –

10  $\mu\text{m}$  [2,15,44] was reported for  $\beta\text{-Ca}_2\text{SiO}_4$  stabilization, i.e., preventing a transformation into  $\gamma\text{-Ca}_2\text{SiO}_4$ .

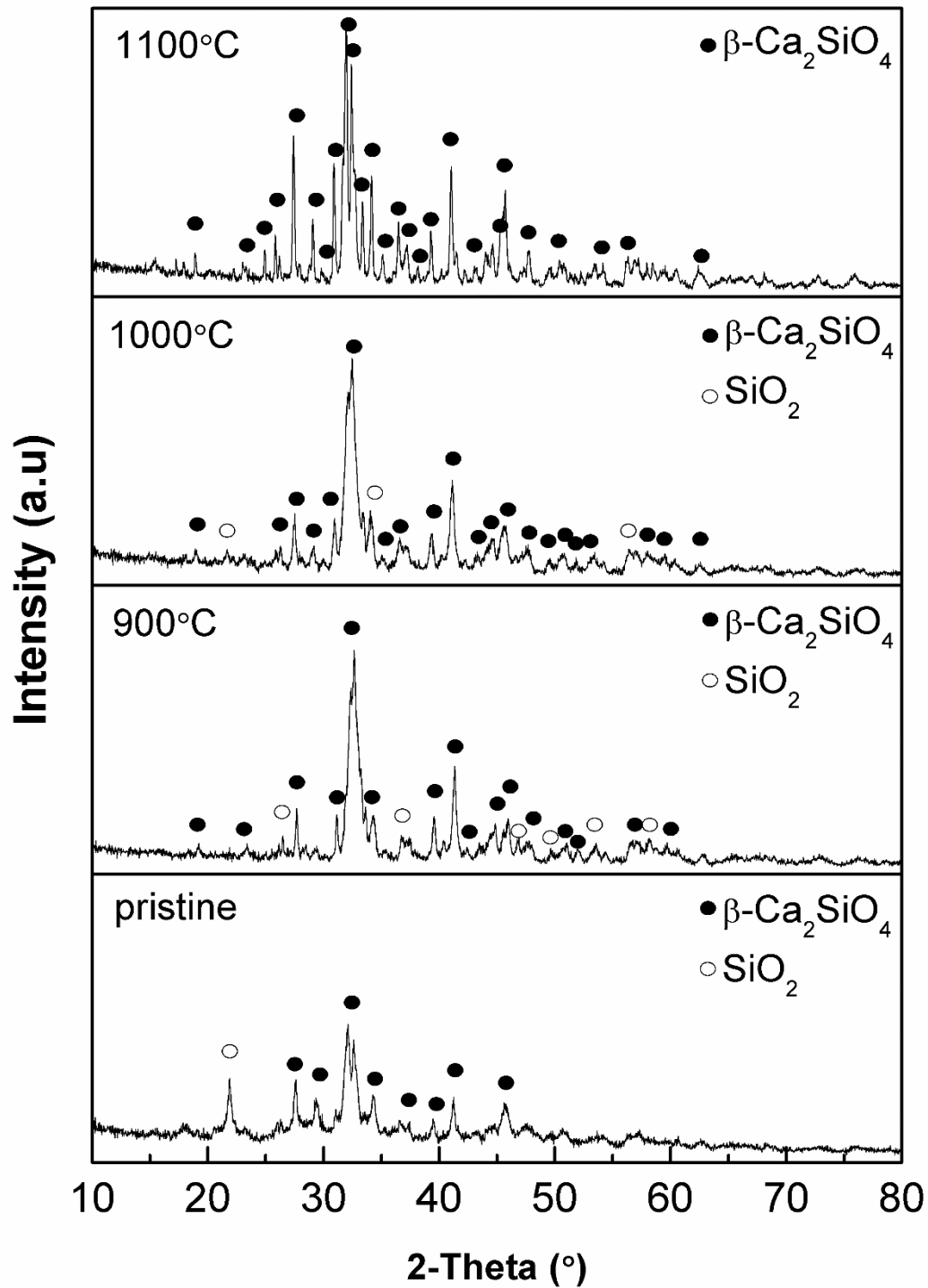


Fig. 3. X-ray diffraction pattern of pristine body and sample sintered at 900°C, 1000°C, and 1100°C.

The XRD Rietveld refinements were carried out to learn more about the effect of sintering temperature on the crystal structure of samples. The obtained refinement parameters are tabulated in Table 3. Refinement reveals  $\beta$ -monoclinic structure with space group (P 121/c1) for samples sintered at different temperatures. The average crystallite size (D) of these sintered ceramics was calculated using the Scherrer formula:

$$D = \frac{0.9\lambda}{\beta \cos\theta} \quad (2)$$

where  $\lambda$  is the wavelength of the incident X-ray,  $\beta$  is the full width at half maximum (FWHM) of the diffraction peak, and  $\theta$  is the Bragg diffraction angle. Table 3 shows that the crystallite size increased drastically from 197 Å at 900°C to 580 Å at 1100°C. All the samples exhibited crystallites in nano-size as measured from XRD. Besides, the values of lattice parameters and cell volume decrease as sintering temperatures rise, which is attributed to lattice relaxation caused by grain size increment. Mohamed *et al.* [34] and Sharma [45] also previously seen similar tendencies. Thus, grain growth might be the reason for an increase in average crystalline size.

The temperature has a significant impact on the lattice properties. From the pristine body to 1000 °C, the  $c/a$  ratio increase indicates the development of ordering and leads to higher crystallinity during sintering. A slight decrease in the  $c/a$  ratio at 1100 °C was attributed to the loss of carbonate ions from the lattice, thereby reducing the lattice distortion. Theoretically, a greater value for the  $c/a$  ratio suggests less cation disorder in the material and is seen favorably for improved electrical properties [46]. A greater  $c/a$  ratio could provide the ions with more space to move in a specific direction in the presence of an electric field, leading to higher energy dipoles that are good for energy storage [47].

**Table 1** The Rietveld Refinement parameter of XRD data for mechanochemical synthesized  $\text{Ca}_2\text{SiO}_4$  samples.

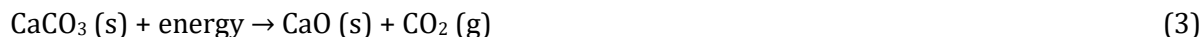
|  | Pristine                                      | 900°C  | 1000°C  | 1100°C  |
|--|---|--|---|---|
| <b>Percentage of <math>\beta</math>-<math>\text{Ca}_2\text{SiO}_4</math> (%)</b> | 82.9  | 90.2   | 96.9  | 100   |
| <b>Space group</b>   | P 121/c1                                      | P 121/c1                                     | P 121/c1                                      | P 121/c1                                      |
| <b>Lattice parameter</b>   | a[Å]=5.50619<br>b[Å]=6.76005<br>c[Å]=10.45987 | a[Å]=5.52401<br>b[Å]=6.7723<br>c[Å]=10.51645 | a[Å]=5.51156<br>b[Å]=6.75872<br>c[Å]=10.49325 | a[Å]=5.50714<br>b[Å]=6.75254<br>c[Å]=10.44811 |
| <b>c/a ratio</b>   | 1.89966                                       | 1.90377                                      | 1.90386                                       | 1.89719                                       |
| <b>Unit cell volume [Å<sup>3</sup>]</b>  | 346.391                                       | 348.2758                                     | 346.5868                                      | 345.2802                                      |
| <b>Bulk density (xrd) [g/cm<sup>3</sup>]</b>                                     | 3.3   | 3.28   | 3.3   | 3.31  |
| <b>Crystallite size [Å]</b>  | 222   | 197  | 199   | 580   |
| <b>Crystal structure</b>   | monoclinic (beta)                             | monoclinic (beta)                            | monoclinic (beta)                             | monoclinic (beta)                             |

### 3.5 Functional group analysis

Fig. 4 shows the FTIR spectra of the studied samples in the wavenumber range of 400 – 4000  $\text{cm}^{-1}$ . This region reveals the presence of functional groups in both pristine and sintered samples. This enables structural analysis of the ceramic material. For the pristine body and sample sintered at 900°C, a peak that appeared between 3200 and 3600  $\text{cm}^{-1}$  is mostly due to the O-H stretching vibration of  $\text{Ca}(\text{OH})_2$ . The formation of  $\text{Ca}(\text{OH})_2$  is due to successive decarbonization and hydration reactions, as shown in Equations (3) and (4). Carbonate,  $\text{CaCO}_3$  decomposed to form  $\text{CaO}$  and  $\text{CO}_2$  upon heat treatment, and then the active  $\text{CaO}$  was further



hydrated by moisture from the atmosphere to form  $\text{Ca(OH)}_2$ , which could not be prevented or avoided.



This demonstrates that the pristine body and sample sintered at  $900^\circ\text{C}$  may chemically react with the surrounding moisture, i.e., water adsorption [48]. Besides, the existence of carbonate,  $\text{CO}_3^{2-}$  groups in the pristine body were detected at the adsorption band of  $1454 \text{ cm}^{-1}$  due to C-O stretching [3], which may be caused by the reaction of CaO with surrounding  $\text{O}_2$  and  $\text{CO}_2$ . After the sintering treatment ( $900\text{--}1100^\circ\text{C}$ ), the intensity band of C-O gradually disappeared due to the decomposition of carbonate to  $\text{CO}_2$  gas [49,50,51]. Apart from that, the wavenumbers of  $1082 \text{ cm}^{-1}$  and  $873 \text{ cm}^{-1}$  for GB,  $874 \text{ cm}^{-1}$  for  $900^\circ\text{C}$ , and  $1000 \text{ cm}^{-1}$  and  $891 \text{ cm}^{-1}$  for both  $1000^\circ\text{C}$  and  $1100^\circ\text{C}$  correspond to bending and stretching Si-O bonds in  $\text{SiO}_4^{4-}$  tetrahedron [48].

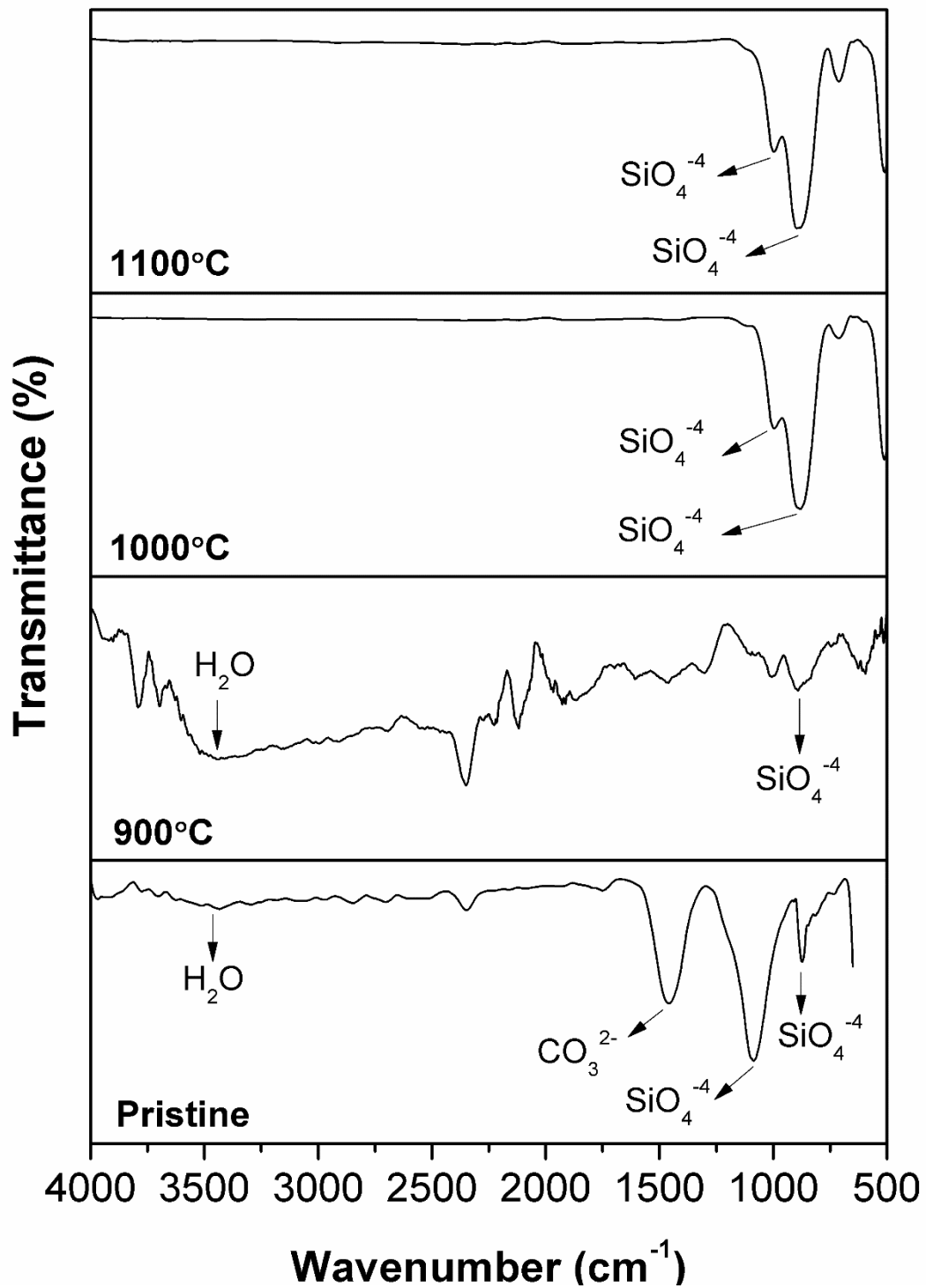


**Fig. 4.** Fourier transform infrared spectra of pristine body, and samples sintered at 900 °C, 1000 °C, and 1100 °C.

### 3.6 Morphological and Physical Analysis

Generally, ceramic sample characteristics are significantly influenced by the sintering temperature. The natural surface SEM micrograph of the pristine body and sintered samples at various sintering temperatures are presented in Fig. 5. It is clearly shown that when the sintering temperature is further increased, larger microcracks are seen distributing at the grain boundaries on the sintered sample's surface. The microcrack formation is not attributed to the intense thermal stress that exacerbates the fracture of adjacent grains during cooling [52,53,54]. It is suggested that the formation of pores induces intergranular cracks. According to the charge compensation mechanism, the oxygen from the carbonate group was decomposed to produce  $\text{CO}_2$  in the ceramic matrix to form pores.

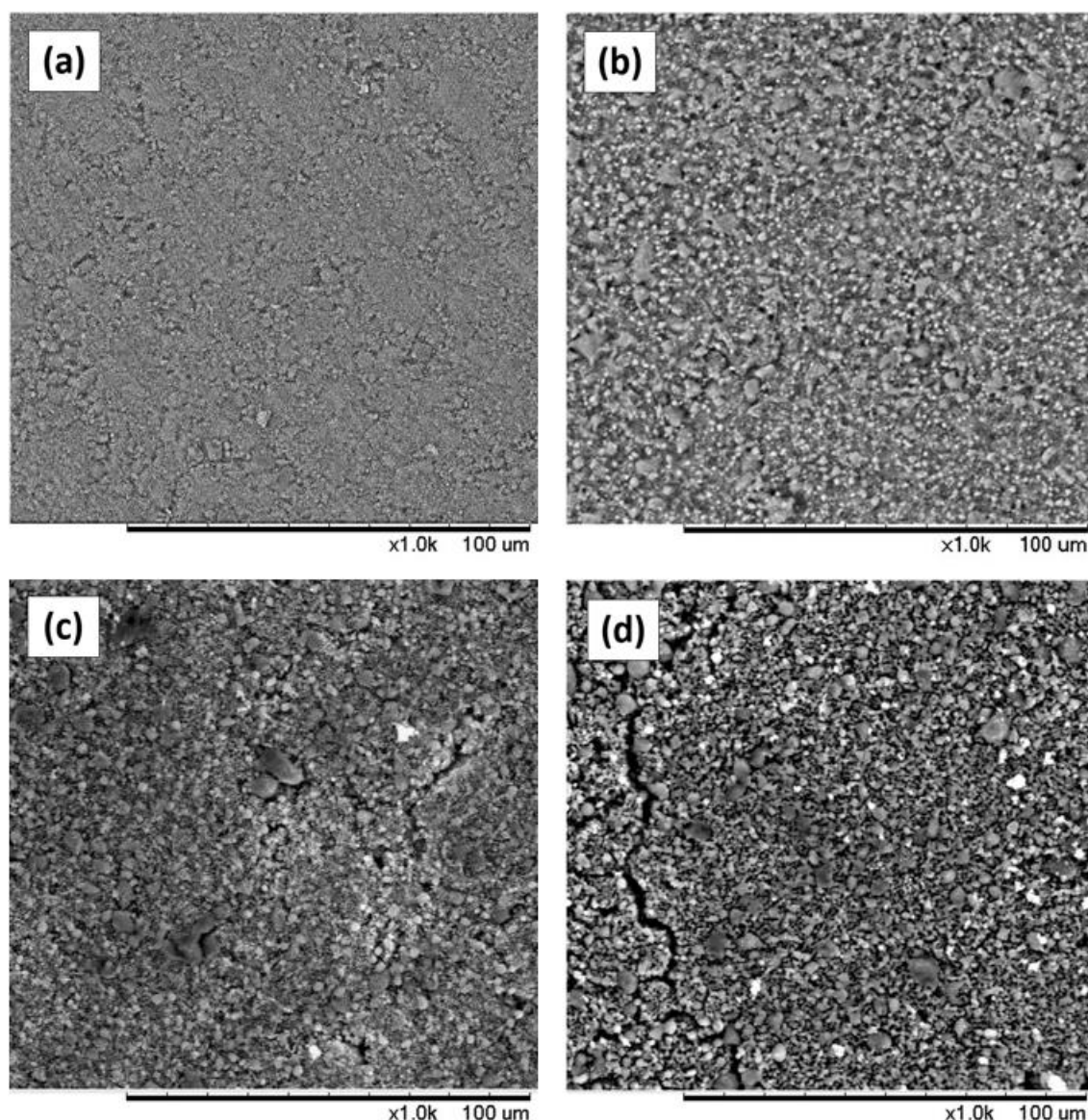


**Fig. 5.** Scanning electron micrograph of (a) pristine body, sample sintered at (b) 900°C (c) 1000°C, and (d) 1100°C.

The volume shrinkage, apparent porosity, and bulk density of the studied samples were measured to characterize the densification behavior. As seen in Table 4, the average grain size

and pore size are clearly correlated with the sintering temperatures. Fig. 6 shows that the apparent porosity increases from 13.8% to 62.5% for the pristine body at 1000 °C. On the contrary, the bulk density has declined from 1.93 g/cm<sup>3</sup> to 1.25 g/cm<sup>3</sup> for the pristine body at 1000 °C. Generally, the progression in bulk density is closely dependent on porosity. However, the relation between the temperatures and bulk density in such a way indicates that at temperatures below 1000 °C the diffusion process cannot be completed. In other words, the firing of the pristine body sample below 1000 °C, is a complicated chemical process with structural evolution and a rise in pore size rather than merely a sintering process with steady densification. Besides, the continuous reaction of the chemical process increased the volume shrinkage of the sample from 3.32% to 23.19%. Raising the temperature to 1100°C has resulted in a denser body as the bulk density increased to 1.34 g/cm<sup>3</sup> while apparent porosity and volume shrinkage decreased to 52.17% and 2.11%, respectively. This is probably due to the fast decomposition of the carbonate group into the gas CO<sub>2</sub>, which gradually destroys the pore structure and contributes to greater densification. In other words, a less porous ceramic is formed as the densification process begins. Moreover, the volume shrinkage decreased with elevating the sintering temperature, which is a common behavior of many conventional porcelain bodies [55,56,57,58]. However, the decrease in shrinkage is contradicted by the increase in bulk density from a macroscopic point of view. Therefore, this has to be thoroughly examined in further studies. Nevertheless, the rich pore properties of ceramic can lead to dramatic changes in performance and applications. This is because porous ceramics have unique properties that could make them useful in a diverse range of applications, from abundant industrial processes to household products.

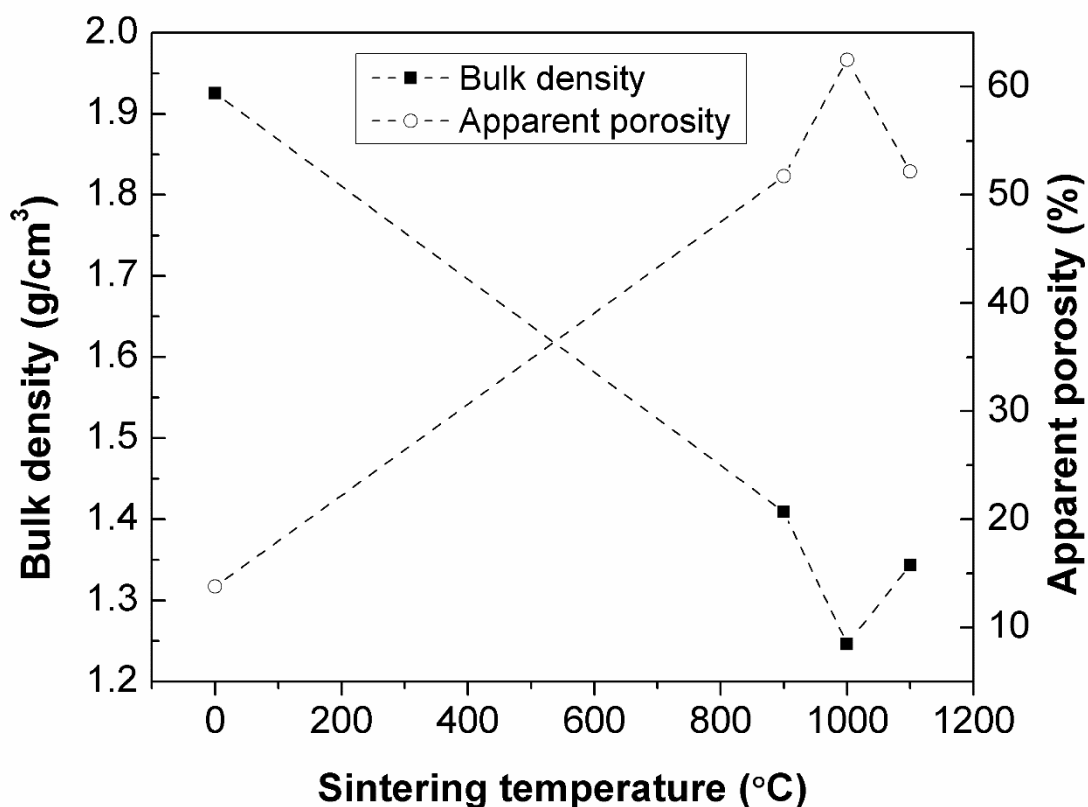


Fig. 6. Bulk density and apparent porosity of samples.

The milling effect should theoretically result in particle agglomeration by increasing the contact area between the particles. Additionally, when the temperature rises, the distance between the

grains' centers decreases, and a grain boundary eventually forms. As seen in Fig. 5(b-c), the grain boundary was not sufficiently formed due to insufficient diffusion during sintering up to 1000°C. However, as seen in Table 4, the average grain size gradually increased with sintering temperature due to grain growth because grain coarsening as a result of diffusion is a thermally activated process. At 1100°C (Fig. 5(d)), the densification and grain growth become more active. The average grain size is approximately 6 µm, with the formation of grain boundaries and necking due to diffusion. From Table 4, the pristine sample is composed of grains with an average size of 3.1123 µm, i.e., less than 10 µm. Its contact points between particles with an irregular microstructure promote slow interdiffusion kinetics when heat treated [52]. When the sintering temperature was increased, the surface of all particles became rough, and the grain size was larger compared with the pristine sample. The changes in the kinetics of movement from boundary to boundary may be the cause of the creation of large grains with irregular forms. This is because grain boundary energy depends on grain boundary orientation and movement [52]. In short, shrinkage, porosity, and density are thought to be the most crucial characteristics of a ceramic body.

**Table 2** Average grain size, pore size, and volume shrinkage.

| Sample   | Average grain size (µm) | Average pore size (µm) | Average volume shrinkage (%) |
|----------|-------------------------|------------------------|------------------------------|
| Pristine | 3.1123                  | 1.6061                 | -                            |
| 900°C    | 3.6841                  | 1.6701                 | 3.32                         |
| 1000°C   | 5.3648                  | 2.2532                 | 23.19                        |
| 1100°C   | 6.0583                  | 2.4504                 | 2.11                         |

#### 4. CONCLUSION

In the present research, pure Ca<sub>2</sub>SiO<sub>4</sub> in β-monoclinic structures with P 121/c1 space group was successfully synthesized through the mechanochemical treatment of a high-speed planetary ball mill using eggshell and rice husk as precursor materials. The mechanochemical technique increased the contact area between the milled particles and exhibited a larger particle size of 801.5 nm due to powder agglomeration induced by the stronger Van Der Waals forces. The effect of sintering temperatures on the physical and morphology properties of the sample was studied. The formation of pores is due to the appearance of CO<sub>2</sub> from the decomposition of CaCO<sub>3</sub> in the consolidated ceramic body. After sintering at the maximum temperature of 1100 °C, 100% Ca<sub>2</sub>SiO<sub>4</sub> in β-monoclinic structures was obtained. The sintered sample is considered to be a high-performance porous ceramic material with a high apparent porosity of 52.17%, a density of 1.34 g/cm<sup>3</sup>, and a volume shrinkage of 2.11%, which is quite competitive in practical applications. Additionally, the sintered Ca<sub>2</sub>SiO<sub>4</sub> samples, without any chemical stabilizer addition, never undergo the dusting phenomenon and remain in shape. This work shows that sintering temperatures have a strong influence on the microstructure, lattice parameter, and crystalline size of the bio-based derived Ca<sub>2</sub>SiO<sub>4</sub>. In short, synthesizing Ca<sub>2</sub>SiO<sub>4</sub> from bio-waste materials would be extremely beneficial to the economy while also addressing environmental pollution concerns.

#### ACKNOWLEDGEMENTS

The author would like to acknowledge the support from the Fundamental Research Grant Scheme (FRGS) under a grant number of FRGS/1/2018/STG07/UNIMAP/02/2) from the Ministry of Higher Education Malaysia. Furthermore, the authors wish to express their gratitude to the Faculty of Electrical Engineering & Technology, and Faculty of Chemistry Engineering & Technology from Universiti Malaysia Perlis (UniMAP) for providing the research facilities. The authors also would like to thank Poh Seng Rice Mill & Co. Sdn. Bhd. for providing the rice husks.

## REFERENCES

- [1] And, S. Z., & Davis, H. M., Observations on Solid-Phase Inversions of Calcium Orthosilicate, Constituent of Dolomite-Silica Brick. *J. Am. Ceram. Soc.* Vol 26, issue 9 (1943) pp.302-307.
- [2] Chan, C. J., Kriven, W. M., & Young, J. F., Physical stabilization of the  $\beta \rightarrow \gamma$  transformation in dicalcium silicate. *J. Am. Ceram. Soc.* Vol 75, issue 6 (1992) pp.1621-1627.
- [3] Yong Tao, Siavash Zare, Fazhou Wang & Mohammad Javad Abdolhosseini Qomi, Atomistic thermodynamics and kinetics of dicalcium silicate dissolution. *Cem. Concr. Res.* Vol 157 (2022) pp.106833.
- [4] Dash, A., Chanda, P., Tripathy, P.K. & Kumar, N., A Review on Stabilization of Ladle Furnace Slag-Powdering Issue. *J. Sustain. Metall.* (2022) pp.1-15.
- [5] Zhang, C., Xu, H., Qing, L., Cai, J., Cheng, X., Huang, S., Dai, B. & Xia, H., Interface characteristics of oil-well cement and rock asphalt coated by dicalcium silicate. *J. Adhes. Sci. Technol.* Vol 35, issue 9 (2021) pp.973-92.
- [6] Gou, Z., & Chang, J., Synthesis and in vitro bioactivity of dicalcium silicate powders. *J. Eur. Ceram. Soc.* Vol 24, issue 1 (2004) pp.93-99.
- [7] Abd El-Hamid, H. K., Abo-Naf, S. M., & Elwan, R. L., Characterization, bioactivity investigation and cytotoxicity of borosilicate glass/dicalcium silicate composites. *J. Non-Cryst. Solids.* Vol 512 (2019) pp.25-32.
- [8] Qianqian, W., Feng, L., Xiaodong, S., Wujun, S., Xuerun, L., Yanhua, G., Shijie, X., & Qing, Z., Relation between reactivity and electronic structure for  $\alpha$ ,  $\alpha'_H$ ,  $\alpha'_L$ ,  $\beta$  and  $\gamma$ -dicalcium silicate: A first-principles study. *Cem. Concr. Res.* Vol 57 (2014) pp.28-32.
- [9] Chehlatt, S., Mezahi, F. Z., Harabi, A., & Oudadesse, H., In vitro hydroxyapatite forming ability of dicalcium silicate prepared from local raw materials and sintered at 1050°C. *Ceramics-Silikáty* Vol 66, issue 3 (2022) pp.167-172.
- [10] Pan, X. L., Lyu, Z. Y., Zhang, C., & Yu, H. Y., Effect of  $\text{Na}_2\text{O}$  on transition and stability of dicalcium silicate based on sintering process. *J. Cent. South Univ.* Vol 29 (2022) pp.1161-1172.
- [11] Chaoqi Shi, Binbin Qian, Qianqian Wang, Franco Zunino, Junying Zhao & Xiaodong Shen, Structure analysis of beta dicalcium silicate via scanning transmission electron microscope (STEM). *Constr. Build. Mater.* Vol 348, issue 19 (2022) pp.128720.
- [12] Muhammad Jawad Ahmed, Remco Cuijpers, Katrin Schollbach, Sieger Van Der Laan, Mary Van Wijngaarden-Kroft, Tiny Verhoeven & Brouwer, H. J. H., V and Cr substitution in dicalcium silicate under oxidizing and reducing conditions – Synthesis, reactivity, and leaching behavior studies. *J. Hazard. Mater.* Vol 442 (2023) pp.130032.
- [13] Qi, C., Xu, X., Wang, D., Feng, Y., Zhang, Q., & Chen, Q., Coverage-dependent adsorption of  $\text{H}_2\text{O}$  on dicalcium silicate (100) surface: A DFT study. *Constr. Build. Mater.* Vol 321 (2022) pp.126403.
- [14] Singh, L., Kim, I. W., Woo, W. S., Sin, B. C., Lee, H. I., & Lee, Y., A novel low cost non-aqueous chemical route for giant dielectric constant  $\text{CaCu}_3\text{Ti}_4\text{O}_{12}$  ceramic. *Solid State Sci.* Vol 43 (2015) pp.35-45.



- [15] Muhammad Jawad Ahmed, Katrin Schollbach, Siegervan der Laan, Miruna Florea & 571rouwers, H. J. H., A quantitative analysis of dicalcium silicate synthesized via different sol-gel methods. *Mater. Des.* Vol 213 (2022) pp.110329.
- [16] Chrysafi, R., Perraki, T.h., & Kakali, G., Sol-gel preparation of  $2\text{CaO}\cdot\text{SiO}_2$ . *J. Eur. Ceram. Soc.* Vol 27, issue 2-3 (2007) pp.1707-1710.
- [17] Tan, Y. N., Liu, Y., Qing, Z., Birdi, G., & Grover, L. M., Synthesis of pure dicalcium silicate powder by the Pechini method and characterization of hydrated cement. In *Materials Science Forum*, Vol 787 (2014) pp.387-394.
- [18] Dimesso, L., Pechini Processes: An Alternate Approach of the Sol-Gel Method, Preparation, Properties and Applications, in: *Handb. Sol-Gel Sci. Technol*, Springer International Publishing, Cham (2016) pp.1-22.
- [19] Restrepo, J.C., Chavarriaga, A., Restrepo, O.J., & Tobón J.I., Synthesis of hydraulically active calcium silicates produced by combustion methods. *MRS Online Proceedings Library (OPL)* Vol 1768 (2015) pp.27-37.
- [20] Pratsinis, S.E., Flame aerosol synthesis of ceramic powders. *Prog. Energy Combust. Sci.* Vol 24, issue 3 (1998) pp.197-219.
- [21] Georgescu, M., Tipan, J., Badanoiu, A., Crisan, D., & Dragan, I., Highly reactive dicalcium silicate synthesized by hydrothermal processing. *Cem. Concr. Compos.* Vol 22, issue 5 (2000) pp.315-319.
- [22] Zhong, H., Wang, L., Fan, Y., He, L., Lin, K., Jiang, W., Chang, J., & Chen, L. Mechanical properties and bioactivity of  $\beta\text{-Ca}_2\text{SiO}_4$  ceramics synthesized by spark plasma sintering. *Ceram. Int.* Vol 37, issue 7 (2011) pp.2459-2465.
- [23] Bouregba, A., & Diouri, A., Potential formation of hydroxyapatite in total blood and dicalcium silicate elaborated from shell and glass powders. *Mater. Lett.* Vol 183 (2016) pp.405-407.
- [24] Choudhary, R., Koppala, S., Srivastava, A., & Sasikumar, S., In-vitro bioactivity of nanocrystalline and bulk larnite/chitosan composites: comparative study. *J. Sol-Gel Sci. Technol.* Vol 74, issue 3 (2015) pp.631-640.
- [25] Smith, D. K., Majumdar, A., & Ordway, F., The crystal structure of  $\gamma$ -dicalcium silicate. *Acta Crystallogr.* Vol 18, issue 4 (1965) pp.787-795.
- [26] Shahsavari, R., Chen, L., & Tao, L., Edge dislocations in dicalcium silicates: Experimental observations and atomistic analysis. *Cem. Concr. Res.* Vol 90 (2016) pp.80-88.
- [27] Liu, X. Y., Tao, S. Y., & Ding, C. X., Bioactivity of plasma sprayed dicalcium silicate coatings. *Biomaterials* Vol 23 (2002) pp.963.
- [28] Roy, D. M., & Oyefesobi, S. O., Preparation of very reactive  $\text{Ca}_2\text{SiO}_4$  powders. *J. Am. Ceram. Soc.* Vol 60 (1977) pp.178.
- [29] Kantro, D. L., & Weise, C. H., Hydration of various beta-dicalcium silicate preparation. *J. Am. Ceram. Soc.* Vol 62 (1979) pp.621.
- [30] Sasaki, K., Ishida, H., Okada, Y., & Mitsuda, T., Highly reactive  $\beta$ -dicalcium silicate: V, influence of specific surface area on hydration. *J. Am. Ceram. Soc.* Vol 76 (1993) pp.870.
- [31] Sandipan Chowdhury, Dipika Dhara, Soumit Chowdhury, Partha Haldar, Kingshuk Chatterjee, & Tapas Kumar Bhattacharya, A novel approach toward microstructure evaluation of sintered ceramic materials through image processing techniques. *Int. J. Appl. Ceram.* Vol 18, issue 3 (2021) pp.773-780.
- [32] JiboHuang, ManwenYao & XiYao, A novel approach to improving the electromechanical properties of PZT-based piezoelectric ceramics via a grain coating modification strategy. *Ceram. Int.* Vol 47, issue 11 (2021) pp.16294-16302.

- [33] Senthil Kumar, R., Sai Priyanka, K.H., Khanra, A.K., & Johnson, R., A novel approach of synthesizing nano  $Y_2O_3$  powders for the fabrication of submicron IR transparent ceramics. *Ceram. Int.* Vol 47, issue 12 (2021) pp.16986-16999.
- [34] Berger, M. B., "The Importance and Testing of Density/Porosity/Permeability/Pore size for Refractories". The Southern African Institute of Mining and Metallurgy Refractories 2010 Conference (2010) pp.110-116.
- [35] Tangboriboon, N., Unjan, W., Sangwan, W., & Sirivat, A., Preparation of anhydrite from eggshell via pyrolysis. *Green Process. Synth.* Vol 7, issue 2 (2018) pp.139-146.
- [36] Nisanart Traipho, Effects of ball milling time and dispersant concentration on properties of a lead zirconate titanate aqueous suspension for tape casting. *J. Ceram. Process. Res.* Vol. 8, issue 2 (2007) pp.137-141.
- [37] Karde, V., Panda S., & Ghoroi C., Surface modification to improve powder bulk behavior under humid conditions. *Powder Technol.* Vol 278 (2015) pp.181-188.
- [38] Amat, N. F., Muchtar, A., Amril, M. S., Ghazali, M. J., & Yahaya, N., Preparation of presintered zirconia blocks for dental restorations through colloidal dispersion and cold isostatic pressing. *Ceram. Int.* Vol 44, issue 6 (2018) pp.6409-6416.
- [39] He, P., Shi, C., Tu, Z., Poon, C. S., & Zhang, J., Effect of further water curing on compressive strength and microstructure of  $CO_2$ -cured concrete. *Cem. Concr. Compos.* Vol 72 (2016) pp.80-88.
- [40] Lu, B., Shi, C., & Hou, G., Strength and microstructure of  $CO_2$  cured low-calcium clinker. *Constr. Build. Mater.* Vol 188 (2018) pp.417-423.
- [41] Zdujić, M., Lukić, I., Kesić, Ž., Janković-Častvan, I., Marković, S., Jovalekić, Č., & Skala, D., Synthesis of  $CaOSiO_2$  compounds and their testing as heterogeneous catalysts for transesterification of sunflower oil. *Adv. Powder Technol.* Vol 30, issue 6 (2019) pp.1141-1150.
- [42] Devi, L. L., Basavapoornima, C., Venkatramu, V., Babu, P. & Jayasankar, C. K., Synthesis of  $Ca_2SiO_4$ :  $Dy^{3+}$  phosphors from agricultural waste for solid state lighting applications. *Ceram. Int.* Vol 43, issue 18 (2017) pp.16622-16627.
- [43] Devi, L. L., Basavapoornima, C., Venkatramu, V., Jayasankar, C. K., Kaewkhao, J. & Lertlop, W., Structural and luminescence properties of  $Sm^{3+}$ -doped  $Ca_2SiO_4$  phosphors from agricultural waste. *Materials Today: Proceedings*, Vol 5, issue 7 (2018) pp.15081-15085.
- [44] Saidani, S., Smith, A., El Hafiane, Y., & Ben Tahar, L., Re-examination of the  $\beta \rightarrow \gamma$  transformation of  $Ca_2SiO_4$ , *J. Eur. Ceram. Soc.* 38 (2018) pp. 4756-4767.
- [45] Sharma, N., Mall, A. K., Gupta, R., Garg, A., & Kumar, S., Effect of sintering temperature on structure and properties of  $GaFeO_3$ . *J. Alloys Compd.* Vol 737 (2018) pp.646-654.
- [46] Xu, Y. (2013). "Ferroelectric materials and their applications", North-Holland, The Netherland, Elsevier, (1991) pp.101-154.
- [47] Gao, F., Dong, X., Mao, C., Cao, F., & Wang, G., c/a Ratio-Dependent Energy-Storage Density in  $(0.9-x)BiO \cdot 5NaO \cdot 5TiO_3-xBaTiO_3-0.1K_0.5NaO \cdot 5NbO_3$  Ceramics. *J. Am. Ceram. Soc.* Vol 94, issue 12 (2011) pp.4162-4164.
- [48] Tan, Y., Liu, Y., Zhang, Z., Hofmann, M., & Grover, L., "Comparing three methods for the synthesis of pure beta-dicalcium silicate". In 2010 4<sup>th</sup> International Conference on Bioinformatics and Biomedical Engineering, (2010, June) pp.1-4. IEEE.
- [49] Almasri, K. A., Matori, K. A., & Zaid, M. H. M., Effect of sintering temperature on physical, structural and optical properties of wollastonite based glass-ceramic derived from waste soda lime silica glasses. *Results in Phys.* Vol 7 (2017) pp.2242-2247.
- [50] Sasmal, N., Garai, M., & Karmakar, B., Preparation and characterization of novel foamed porous glass-ceramics. *Mater. Charact.* Vol 103 (2015) pp.90-100.



- [51] Jusoh, W. N. W., Matori, K. A., Zaid, M. H. M., Zainuddin, N., Khiri, M. Z. A., Rahman, N.A.A., Jalil, R.A. & Kul, E., Effect of sintering temperature on physical and structural properties of Alumino-Silicate-Fluoride glass ceramics fabricated from clam shell and soda lime silicate glass. *Results in Phys.* Vol 12 (2019) pp.1909-1914.
- [52] Kamil Kornaus, Izabela Czekaj, Natalia Sobuś, Radosław Lach, & Agnieszka Gubernat, Remarkable Structural Modifications of Tialite Solid Solutions Obtained by Different Methods. *Materials*, vol 15, issue 11 (2022) pp.3981.
- [53] Dittert, B., Wiessner, M., Angerer, P., Lackner, J.M., & Leichtfried, H., Tailored Al<sub>2</sub>O<sub>3</sub>-Al<sub>2</sub>TiO<sub>5</sub>-TiO<sub>2</sub> Composite Ceramics from Different Titanium Precursors, *Arch. Metall. Mater.* Vol 64, issue 4 (2019) pp.277-1286.
- [54] Jiawei Lian, Qingliang Shan, Weiwei Chen, Qian Ma, Shenghui Zeng, Hao Xiong, Yewei Wang, Qiankun Xu, & Anze Shui, Influence of Cooling Rates on the Microstructure and Mechanical Properties of Aluminum Titanate Flexible Ceramic. *Adv. Eng. Mater.* Vol 23, issue 9 (2021) pp.2100170
- [55] Maity, S. & Sarkar, B. K., Development of high-strength whiteware bodies. *J. Eur. Ceram. Soc.* Vol 16, issue 10 (1996) pp.1083-1088.
- [56] Carbajal, L., Rubio-Marcos, F., Bengochea, M. A. & Fernandez, J. F., Properties related phase evolution in porcelain ceramics. *J. Eur. Ceram. Soc.* Vol 27, issue 13-15 (2007) pp.4065-4069
- [57] Martin-Marquez, J., Rincon, J. Ma., & Romero, M., Effect of firing temperature on sintering of porcelain stone ware tiles. *Ceram. Int.* Vol 34, issue 8 (2007) pp.1867-1873.
- [58] Tian, X., Günster, J., Melcher, J., Li, D., & Heinrich, J. G., Process parameters analysis of direct laser sintering and post treatment of porcelain components using Taguchi's method. *J. Eur. Ceram. Soc.* Vol 29, issue 10 (2009) pp.1903-1915.

